Liquid Drop Growth on a Fiber

A. L. Yarin
Faculty of Mechanical Engineering, Technion–Israel Institute of Technology, Haifa 32000, Israel

G. G. Chase
Dept. of Chemical Engineering, The University of Akron, OH 44325

W. Liu, S. V. Doiphode, and D. H. Reneker
Maurice Morton Institute of Polymer Science, The University of Akron, OH 44325

DOI 10.1002/aic.10661
Published online September 13, 2005 in Wiley InterScience (www.interscience.wiley.com).

A quantitative model is described and verified to predict the growth of oil droplets by coalescence on a single nanofiber. The model considers a stream of fluid carrying many tiny droplets of a different fluid. The mechanisms by which the tiny droplets are captured by a drop growing on a fiber are considered. Different capture mechanisms are examined, including interception, Brownian motion of droplets, and vapor deposition by diffusion. It is shown that droplet interception and Brownian diffusion contribute to drop growth on nanofibers for airborne oil droplets in the size range from 100 to 1000 nm. Merging of growing drops on the fiber is also modeled and experimentally observed. © 2005 American Institute of Chemical Engineers *AIChE J,* 52: 217–227, 2006
Keywords: drops, fibers, nanofibers, electrospinning, coalescence, filtration

Introduction

Coalescing filters are used to remove immiscible droplets from fluid streams. Removal of water droplets from gasoline or aviation fuels provides an example. Coalescing filters are also used to remove small liquid droplets from gases. Coalescing filters (also called de-misters) are used for cleaning indoor air in large buildings, for capture and recycle of liquid droplets produced by industrial operations, for cleaning of exhaust gases from industrial chemical reactors and cleaning of restaurant kitchen fryer exhausts, and for preventing fine droplets of lubricants from entering computer hard-disk enclosures.

The present article predicts the capture of oil droplets from an airstream by microfibers or nanofibers and predicts the growth of drops on the fibers. Nanofibers are of interest because of their potential to enhance capture efficiency of submicron droplets. The nanofibers used in this work are produced by electrospinning of polymer solutions.[1-3]

Note that herein the term *droplet* refers to a liquid particle present in the gas flow stream and the term *drop* refers to a liquid particle attached to a fiber. Droplets are captured by the fibers and the drops on the fiber grow as they capture more droplets. The main steps in the coalescence filtration process are (1) transport of small droplets in an immiscible fluid to the filter, (2) attachment of small droplets to the surface of fibers, (3) increase in size of drops on the fiber, (4) merging and transport of drops on the fiber, and (5) removal of the drops from the filter.[4] The smallest drops may have clamshell attachment, which changes to a bead as more or large droplets are captured, although this process cannot be followed in the optical micrographs. By the time the drops are large enough to be observed they are spherical beads.

Single collector capture mechanisms collect each droplet in one event, at one point on a fiber, on a granular particle or on the surfaces of a pore. Multifiber capture mechanisms such as straining, pore bridging, and pore blocking are not considered in this study. Efficiency prediction methods in aerosol filtration are well developed.[4-7] Various models for drop coalescence and drainage are discussed by Sherony et al.,[4] Sareen et al.,[8] Spielman and Goren,[9] Bitten,[10] Rosenfeld and Wasan,[11] Briscoe et al.,[12] and Raynor and Leith.[13] Predictions of overall filter performance model of individual collection mechanisms is the

sum of several dominant collection mechanisms. Raynor and Leith[13] combined several mechanisms to model the effect of accumulated liquid on the filter performance. Most of these models were developed to predict only filter efficiency.

Briscoe et al.[12] presented images of growing and merging oil drops on microfibers in a continuous water phase. Aramid fibers with a diameter of 7 μ were used. A simple physical model was proposed to explain the influence of coalescence processes on drop growth. Their model predicts that the growth rate of drop diameter ($2a$) is inversely proportional to the drop diameter. The drop radius a is proportional to $t^{1/2}$, where a is the drop radius and t is the time.

An aerosol droplet is assumed to be captured rapidly if a droplet touches a fiber or the surface of the collected fluid, which is usually a larger drop. The interception type of mechanism occurs when a droplet of a finite diameter follows a streamline (in a steady-state flow field) and touches the fiber or a drop. In the Brownian diffusion capture mechanism, the Brownian motion moves droplets from one streamline to another. The inertial type of capture occurs when the inertia of a droplet causes the droplet to depart from a streamline, impact the fiber or a drop, and then be captured.

This report describes an extensive model of growth of oil drops on a single fiber based on hydrodynamics of the two-phase stream flowing past the fiber. Both potential and creeping flows are considered. In potential flow[14] the velocity is the gradient of a scalar potential function. A potential flow is steady, irrotational, and the fluid is inviscid. In creeping flow[15] viscous forces dominate the inertial forces, as indicated by the Reynolds number $\mathrm{Re} < 1$, and the fluid is viscous. Interception, Brownian motion, and vapor deposition by diffusion mechanisms for droplet deposition are considered. The inertial impaction type of capture mechanism is not considered herein because the Stokes number for the fibers and droplet sizes considered in this study was calculated to be about 0.003. For this Stokes number the capture efficiency arising from inertial impaction is only about 1.6×10^{-7} compared to interception mechanism, which is of the order of 1.

In the two sections that follow interception based on potential flow and on creeping flow of the gas are modeled. In the next three sections models are derived for the Brownian motion of the droplets; the vapor deposition of the liquid molecules onto a growing drop as a possible mechanism of liquid accumulation in the drop; and the merging of two neighboring drops on a fiber, leading to the sudden appearance of a bigger drop, which may be blown off the fiber or removed by movement along the fiber. The next two sections include a discussion of the experiments and a comparison of the theoretical results to the experimental data. Conclusions are drawn in the last section of the paper.

Drop Growth on a Single Fiber: Potential Flow with Interception

Consider potential flow with tiny spherical droplets of radius δ. Droplet concentration is denoted by c (c is measured in droplets/m^3). The fiber is normal to the x-axis at $x = 0$. The direction of the fiber defines the z-axis (Figure 1). The flow velocity along the x-axis is $-U$. Assume that at time τ a droplet is intercepted by the fiber (see Figure 1). A droplet is said to be intercepted by the fiber when the droplet following a streamline

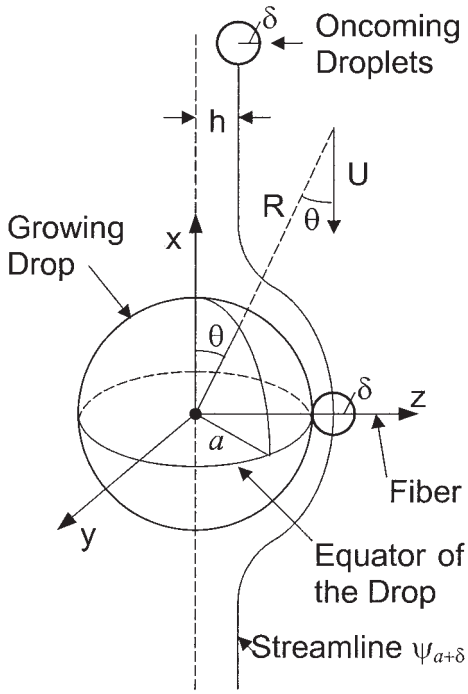

Figure 1. Drop of radius $a(t)$ growing on a fiber in two-phase flow.

The oncoming droplets are carried by fluid flow in the $-x$ direction, toward a growing drop.

touches the fiber surface and attaches to the fiber. Other oncoming droplets are subsequently intercepted and the drop on the fiber grows. In the present section the drop growth rate is modeled and its current radius is calculated as a function of time. Note that those oncoming droplets that are not intercepted by existing drops but do deposit on a fiber will give rise to other growing drops. Transport of liquid between the captured drops on the fiber by a film mechanism is neglected in the present section because there is no evidence that such films exist in our experiments.

In the present work we deal with droplets in the range of 100 to 1000 nm and drops growing on nanofibers (333 nm in diameter) of the order of 1.5 μm. It is emphasized that it was demonstrated in the literature that continuum-like flow patterns and continuum-based approaches to their description are fully valid in this size range.[3,16-18]

Considering the flow around a larger growing drop on the fiber, we neglect the effect of the fiber because we assume that the drop grows rapidly to a diameter much larger than the fiber diameter. The Reynolds number [$\mathrm{Re} = U2a/\nu$] is significantly greater than one ($\mathrm{Re} \gg 1$) in the present section. The drop radius is a and ν is the kinematic viscosity of the gas. The general structure of the flow field can be represented as an inviscid potential flow (that is, neglecting viscous effects). The flow is axisymmetric around the x-axis of the drop, assuming only minor local effects from the fiber that supports the growing drop. The corresponding stream function ψ is given as[19]

$$\psi = -\frac{1}{2} UR^2 \sin^2\theta \left(1 - \frac{a^3}{R^3}\right) \tag{1}$$

where R and θ are the spherical coordinates (Figure 1).

The corresponding velocity components are found as

$$v_R = \frac{1}{R^2 \sin\theta}\frac{\partial\psi}{\partial\theta} \tag{2}$$

$$v_\theta = -\frac{1}{R\sin\theta}\frac{\partial\psi}{\partial R} \tag{3}$$

The values of the stream function at the drop equator are obtained from Eq. 1 by substituting $\theta = \pi/2$

$$\psi|_{\theta=\pi/2} = -\frac{1}{2}UR^2\left(1 - \frac{a^3}{R^3}\right) \tag{4}$$

At the equator the streamlines approach the drop surface closer than at any other cross-section. Therefore all the oncoming droplets, whose centers are within the streamline, $\psi_{a+\delta} = \psi(R = a + \delta, \theta = \pi/2)$ will be intercepted by the growing drop. Substituting for R in Eq. 4, we obtain

$$\psi_{a+\delta} = -\frac{1}{2}U(a+\delta)^2\left[1 - \frac{a^3}{(a+\delta)^3}\right] \tag{5}$$

The surface of the growing drop, $R = a$, according to Eq. 1, corresponds to the streamline

$$\psi_a = 0 \tag{6}$$

Volumetric flow rate Q of gas between the streamlines $\psi_{a+\delta}$ and ψ_a in the equatorial cross section is given by

$$Q = \left|\int_a^{a+\delta} v_\theta|_{\theta=\pi/2} 2\pi R dR\right| \tag{7}$$

Substituting v_θ from Eq. 3 in the above equation we find

$$Q = \left|\int_a^{a+\delta}\left(-\frac{1}{R}\frac{\partial\psi}{\partial R}\right)\Bigg|_{\theta=\pi/2} 2\pi R dR\right| = 2\pi|\psi_a - \psi_{a+\delta}| \tag{8}$$

Based on Eqs. 5–8, we obtain

$$Q = 2\pi\frac{1}{2}U(a+\delta)^2\left[1 - \frac{a^3}{(a+\delta)^3}\right] \tag{9}$$

Also we know that for a circular cross-section

$$Q = \pi h^2 U \tag{10}$$

where h is the cross-sectional radius of the stream tube corresponding to the streamline $\psi_{a+\delta}$ at infinity. Combining Eqs. 9 and 10, we find

$$h = (a+\delta)\sqrt{1 - \frac{a^3}{(a+\delta)^3}} \tag{11}$$

Because the growing drop rapidly becomes much larger than the oncoming droplets, we assume $\delta \ll a$ and then Eq. 11 reduces to

$$h = \sqrt{3\delta a} \tag{12}$$

The mass flux of the oncoming droplets intercepted by the growing drop during time dt is given by

$$dJ = \pi h^2 U dt c \rho_\ell \frac{4}{3}\pi\delta^3 \tag{13}$$

where ρ_l is the liquid density.

The mass balance describing the growth rate of the drop on the fiber is given by

$$d\left(\rho_\ell \frac{4}{3}\pi a^3\right) = dJ \tag{14}$$

Substituting Eqs. 12 and 13 in Eq. 14, we obtain

$$a\frac{da}{dt} = \pi U c \delta^4 \tag{15}$$

Integrating Eq. 15 using the initial condition $a = \delta$ at $t = \tau$ we obtain

$$a = \delta\sqrt{1 + 2\pi U c \delta^2 (t - \tau)} \tag{16}$$

Drop Growth on a Single Fiber: Creeping Flow with Deposition of Droplets by Interception

In the case of $\mathrm{Re} < 1$, the flowfield cannot be described as a potential flow as was done in the previous section. Then the stream function of Eq. 1 is replaced by the one for the corresponding low Reynolds number creeping flow as follows[19]

$$\psi = -\frac{1}{2}UR^2\sin^2\theta\left(1 - \frac{3}{2}\frac{a}{R} + \frac{a^3}{2R^3}\right) \tag{17}$$

Substituting $R = (a + \delta)$ and $\theta = \pi/2$ in Eq. 17, we obtain

$$\psi_{a+\delta} = -\frac{1}{2}U(a+\delta)^2\left[1 - \frac{3}{2}\frac{a}{(a+\delta)} + \frac{a^3}{2(a+\delta)^3}\right] \tag{18}$$

As before, in Eq. 6, $\psi_a = 0$.

From Eqs. 7, 8, and 18 we obtain

$$Q = 2\pi\frac{1}{2}U(a+\delta)^2\left[1 - \frac{3}{2}\frac{a}{(a+\delta)} + \frac{a^3}{2(a+\delta)^3}\right] \tag{19}$$

Q is also given by Eq. 10. Then, using Eqs. 10 and 19 we obtain

$$h = (a + \delta)\sqrt{1 - \frac{3}{2}\frac{a}{(a+\delta)} + \frac{a^3}{2(a+\delta)^3}} \tag{20}$$

In the limit, when the oncoming droplets are much smaller than the growing drop, $\delta \ll a$, we obtain from Eq. 20

$$h = \sqrt{\frac{3}{2}}\,\delta \tag{21}$$

Comparing this result with the one for the potential flow given by Eq. 12, we see that the interception zone has been reduced in creeping flow. Indeed, denoting $h_p = \sqrt{3\delta a}$ and $h_c = \sqrt{3/2}\delta$ and, because we assume that $\delta \ll a$, we find

$$h_c \ll h_p \tag{22}$$

This result corresponds to the fact that the flow displacement from the droplet surface is stronger in creeping than in the potential flow.

Using Eqs. 13, 14, and 21, we find that the growth rate of the drop on the fiber is

$$a^2\frac{da}{dt} = \frac{\pi}{2}Uc\delta^5 \tag{23}$$

Integrating Eq. 23, we obtain an expression for the drop radius as a function of time

$$a = \delta\left[1 + \frac{3\pi}{2}Uc\delta^2(t - \tau)\right]^{1/3} \tag{24}$$

Drop Growth on a Single Fiber: Creeping Flow with Deposition of Droplets by Brownian Diffusion

Deposition by Brownian motion may be the most important mechanism for capture of submicron particles. In the creeping flow regime the deposition rate on a sphere is characterized by the relation between Sherwood (Sh) and Peclet (Pe) numbers[20] as follows

$$\mathrm{Sh} = 1 + (1 + \mathrm{Pe})^{1/3} \tag{25}$$

which is uniformly valid in the range $0 \le \mathrm{Pe} \le 10^4$. Here the Sherwood and the Peclet numbers are defined as

$$\mathrm{Sh} = \frac{h_m 2a}{D} \tag{26}$$

$$\mathrm{Pe} = \frac{U2a}{D} \tag{27}$$

where h_m is the mass transfer coefficient, D is the diffusion coefficient attributed to Brownian motion, and a is the radius of the growing drop.

The droplet diffusion coefficient is given by the Einstein formula as follows

$$D = \frac{kT}{6\pi\mu\delta} \tag{28}$$

where k is the Boltzmann constant, T is the temperature, and μ is the viscosity of the surrounding gas.

In creeping flow with $\mathrm{Re} < 1$ the Peclet number [$\mathrm{Pe} = U2a/D$] can be large or small. In the limit of $\mathrm{Pe} \gg 1$, we obtain from Eqs. 25–27

$$\frac{h_m 2a}{D} = \left(\frac{U2a}{D}\right)^{1/3} \tag{29}$$

Alternatively in the case of $\mathrm{Pe} \to 0$

$$\frac{h_m 2a}{D} = 2 \tag{30}$$

The corresponding expressions for the mass-transfer coefficient for $\mathrm{Pe} \gg 1$ and $\mathrm{Pe} \to 0$ are

$$h_m = \frac{D^{2/3}}{(2a)^{2/3}}U^{1/3} \tag{31}$$

$$h_m = \frac{D}{a} \tag{32}$$

In terms of the mass-transfer coefficient the mass balance equation for the growing drop is

$$\frac{d}{dt}\left(\rho_\ell\frac{4}{3}\pi a^3\right) = 4\pi a^2 h_m\left(c\rho_\ell\frac{4}{3}\pi\delta^3\right) \tag{33}$$

In the case of $\mathrm{Pe} \gg 1$ using Eqs. 31 and 33, we obtain

$$\frac{da^{5/3}}{dt} = \frac{20}{9}\frac{\pi}{2^{2/3}}(c\delta^3)D^{2/3}U^{1/3} \tag{34}$$

which yields after integration

$$a = \delta\left[1 + \frac{20}{9}\frac{\pi}{2^{2/3}}c\delta^{4/3}D^{2/3}U^{1/3}(t - \tau)\right]^{3/5} \tag{35}$$

In the case of $\mathrm{Pe} \to 0$, using Eqs. 32 and 33, we obtain

$$\frac{da^2}{dt} = \frac{8\pi}{3}Dc\delta^3 \tag{36}$$

which yields after integration

$$a = \delta\left[1 + \frac{8\pi}{3}Dc\delta(t - \tau)\right]^{1/2} \tag{37}$$

Thus, in creeping flow with Brownian diffusion, Eqs. 35 and 37 give the two limiting case models, for $\mathrm{Pe} \gg 1$ and for $\mathrm{Pe} \to 0$, respectively.

Drop Growth on a Fiber: Creeping Flow with Molecular Deposition Driven by Diffusion

Single molecules or molecular clusters may sometimes be present in the fluid stream and contribute to the drop growth. Because of this we consider here the rate of drop growth arising from vapor deposition. Vapor deposition is characterized by the vapor diffusion coefficient D_v. In the present case the dependency of the Sherwood number on the Peclet number (Eq. 25) still holds, as well as the expressions for the mass transfer coefficient h_m given by Eqs. 31 and 32. Therefore we have in the limits of Pe $\gg 1$ and Pe $\to 0$ expressions for h_m respectively as follows

$$h_m = \frac{D_v^{2/3}}{(2a)^{2/3}} U^{1/3} \tag{38}$$

$$h_m = \frac{D_v}{a} \tag{39}$$

The mass balance of Eq. 33 is now replaced by

$$\frac{d}{dt}\left(\rho_\ell \frac{4}{3}\pi a^3\right) = 4\pi a^2 h_m(\rho_\ell c_1) \tag{40}$$

where c_1 is the volume fraction of vapor in the gas flow.

In the case of Pe $\gg 1$, using Eqs. 38 and 39, we obtain

$$\frac{da^{5/3}}{dt} = \frac{5}{3}\frac{D_v^{2/3}}{2^{2/3}} U^{1/3} c_1 \tag{41}$$

which yields after integration with the initial condition, $a = 0$ at $t = \tau$

$$a = \left[\frac{5}{3}\frac{D_v^{2/3}}{2^{2/3}} U^{1/3} c_1 (t - \tau)\right]^{3/5} \tag{42}$$

In the case of Pe $\to 0$, using Eqs. 39 and 40, we obtain

$$\frac{da^2}{dt} = 2D_v c_1 \tag{43}$$

which yields after integration

$$a = \sqrt{2D_v c_1 (t - \tau)} \tag{44}$$

Thus, in creeping flow with molecular diffusion, Eqs. 42 and 44 give the two limiting case models, for Pe $\gg 1$ and for Pe $\to 0$, respectively.

Merging of Two Neighboring Drops on a Fiber

Experimental data suggest that growth of a drop on a fiber can be changed abruptly when a drop is blown along or off the fiber. This can happen when the drops become too large to withstand the air drag. One of the reasons that a drop becomes too large arises from its monotonic growth as tiny droplets, which are collected from the flowing fluid. Another reason is the sudden merging with a neighboring drop. This results in the appearance of a bigger combined drop, which is more likely to be blown along or off the fiber because of its large size. The present section is devoted to the analysis of the merging of two adjacent drops on a fiber.

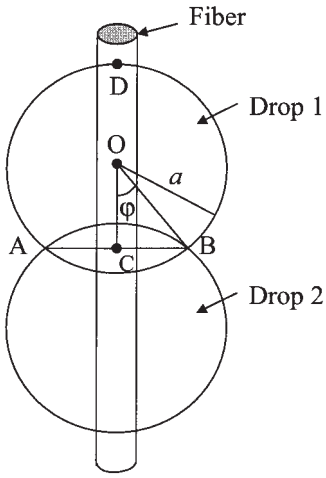

Figure 2. Two drops merging on a fiber.

Merging is attributed to the action of surface tension when the drops touch each other. The contact can be caused by the monotonic drop growth. Contact can also result from the displacement of a drop along the fiber because of a velocity component of the gas flow parallel to the fiber. No evidence of contact through a thin film on the fiber was observed. In the present section the characteristic merging time after contact of adjacent drops is modeled.

Consider two drops on a fiber with an established small contact area AB between them (Figure 2). The drops are assumed to be equal and the fiber to be small enough to neglect its effect on the developing flow. We approximate the drop by a sphere of radius a, which is time dependent. To find $a(t)$ we express the volume of the compound two-drop system V as the volume of two spherical segments (one of them is denoted as ABD in Figure 2, and the other has an equal volume). This yields

$$V = 2\frac{1}{3}\pi h^2(3a - h) = 2\frac{4}{3}\pi a_0^3 \tag{45}$$

and

$$h = a + a\cos\varphi \tag{46}$$

where h is the length of DC in Figure 2. The drop radius at the beginning of merging is denoted a_0. The angle $\varphi(t)$ is defined in Figure 2.

By substituting Eq. 46 in Eq. 45, we obtain

$$\frac{2}{3}\pi a^3(1 + \cos\varphi)^2(2 - \cos\varphi) = \frac{8}{3}\pi a_0^3 \tag{47}$$

For small enough contact areas the angle is small, that is, $\varphi \ll 1$ and $\cos\varphi = 1 - \varphi^2/2$. Using this expansion in Eq. 47, we

find that the lefthand side is equal to $(8\pi a^3/3) + O(\varphi^4)$. Therefore Eq. 47 reduces to

$$\frac{8\pi}{3} a^3 + O(\varphi^4) = \frac{8\pi}{3} a_0^3 \tag{48}$$

As before, neglect the terms $O(\varphi^4)$ and thus obtain

$$a \approx a_0 \tag{49}$$

which means that the drop radius is approximately constant during the merging process.

Flow velocity v, inside the drops, is of the order of $|dh/dt|$. Therefore

$$v = \frac{a_0}{2} \frac{d\varphi^2}{dt} \tag{50}$$

where we used Eq. 46 and approximated sin φ by φ.

The rate of strain in the drops $\dot{\varepsilon} = v/a_0$ and from Eq. 50 we find that $\dot{\varepsilon}$ is of the order of $(1/2)d\varphi^2/dt$. Therefore the viscous dissipation rate is given by

$$E_d = \frac{16\pi}{3} \mu_\ell a_0^3 \left[\frac{d}{dt} \left(\frac{\varphi^2}{2} \right) \right]^2 = 2\mu_\ell \frac{8\pi a_0^3}{3} \dot{\varepsilon}^2 \tag{51}$$

The surface energy is given by

$$E_s = \sigma 2(2\pi a h) \tag{52}$$

where σ is the surface tension coefficient.

By substituting Eqs. 46 and 49 in Eq. 52 and accounting for the fact that $\varphi \ll 1$ we obtain

$$E_s = \sigma 4\pi a_0^2 \left(2 - \frac{\varphi^2}{2} \right) \tag{53}$$

When the viscous effects are dominant and the inertial effects are neglected, the energy balance is given by

$$E_d = -\frac{dE_s}{dt} \tag{54}$$

Substituting Eqs. 51 and 53 in Eq. 54, we obtain

$$\frac{d\varphi^2}{dt} = \frac{3\sigma}{2\mu_\ell a_0} \tag{55}$$

Integrating the above differential equation we obtain

$$\varphi = \sqrt{\frac{3\sigma}{2\mu_\ell a_0}}\, t^{1/2} \tag{56}$$

Also, for the radius of the contact area CB (Figure 2) denoted r_c and equal to $a \sin \varphi \approx a_0\varphi$, we obtain

$$r_c = a_0 \sqrt{\frac{3\sigma}{2\mu_\ell a_0}}\, t^{1/2} \tag{57}$$

and the estimate for the merging time t_* as

$$t_* = \frac{2\mu_\ell a_0}{3\sigma} \tag{58}$$

Note that Eqs. 56–58 were obtained by Frenkel[21] in his seminal work on viscous sintering.

The *Ohnesorge number* (Oh), as defined by Boucher and Alves,[22] is the ratio of the viscous forces to the inertial and surface tension forces

$$\mathrm{Oh} = \frac{\mu_\ell}{\sqrt{\rho_\ell \sigma a_0}} \tag{59}$$

For oil $\rho_l = 835$ kg/m^3, $\sigma = 23.65 \times 10^{-3}$ kg/s^2, $a_0 \leq 10^{-5}$ m, and $\mu_l = 1$ kg m^{-1} s^{-1}, the Ohnesorge number is $\mathrm{Oh} = 54.8 \gg 1$. Therefore in this case the viscous forces are dominant and Eq. 58 is appropriate.

Note also that drops of the order of 0.1 to 10 μm are big enough not to be prone either to line tension (the effect is of importance only at the few Angstroms[23]) or to such thermodynamic effects as the Kelvin effect (the enhancement of evaporation rate over curved surfaces[24]). Therefore, the above continuum description fully holds for them.

Experimental Description

For this study, oil droplets were generated by heating oil in a pot and mixing the evaporated oil molecules with an air stream flowing through the pot. The resulting suspension of oil droplets in air was passed through the filter where droplets were captured on nanofibers. The diameter of merging drops on polymer nanofibers and their growth rate were observed microscopically as a function of time.

Preparation of nanofiber network

Nanofibers of poly(meta-phenylene isophthalamide), called MPD-I or Nomex®, were prepared by an electrospinning process.[3,25,26] Nomex® fibers ($M_w = 90{,}000$ g/mol) were obtained from the Dupont Company. The fibers were dissolved in *N,N*-dimethylacetamide containing 4% lithium chloride at 60°C to form a homogeneous solution with 16% polymer concentration. The solution was filtered to remove any particles. During electrospinning, the polymer solution was held in a glass pipette. When a high voltage was applied through a copper wire in electrical contact with the solution, a charged liquid jet emerged from a liquid drop at the tip of the pipette. As the jet traveled in air, the solvent evaporated, leaving behind a charged polymer fiber. Continuous fibers of average diameter 333 nm were collected as a thin nonwoven fiber network. The spinning voltage was in the range of 15 to 25 kV with the collector about 20 cm from the tip of the pipette.

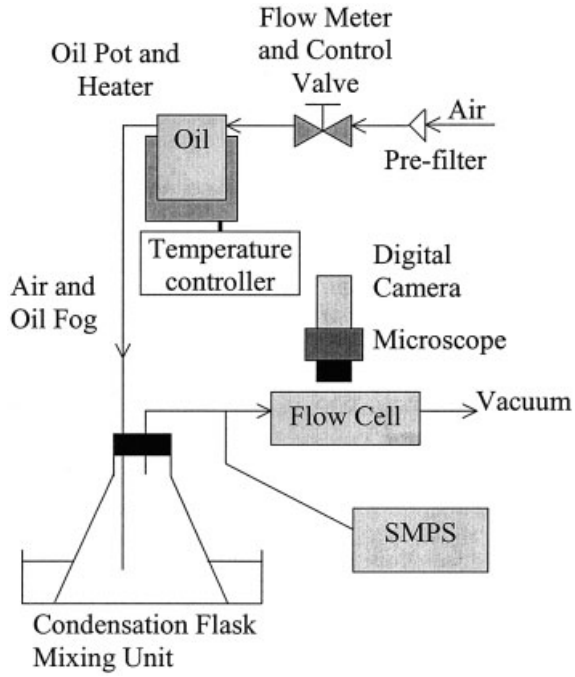

Figure 3. Experimental setup used for observation of accumulation of oil droplets on nanofibers.

The filter cell and microscopic observation of nanofibers

Figure 3 is the experimental setup used. Air was passed through a pre-filter to remove solid and liquid impurities present in the air stream. A valve on a rotameter was used to measure and control air flow rate to the oil pot at 0.1 L/min. The inlet pressure in the flow stream was approximately 1 atmosphere. Mineral oil was placed in the oil pot. The oil pot temperature was controlled with a digital temperature controller (Omron E5EN). Air flowed through the oil pot and carried the oil fog to a flask (the length of a small-diameter plastic tube between the pot and the flask was about 0.7 m), which captured any large droplets present in the fog. The flask also acted as a mixing chamber before sending the air stream by a 0.34 m long small-diameter tube through the filter cell. The flow path through a 3-mm plastic tube and the flask was about 1 m long and mostly at room temperature. The fog, containing only tiny oil droplets and an insignificant concentration of evaporated oil molecules, passed through a fiber network, which was observed at a high magnification with an optical microscope. The growth of individual oil drops on a nanofiber was observed using white light, epi-illumination, and a 40 $\times$ objective lens. Video images were recorded with a Sony Digital Camcorder (DCR-TRV20).

The distribution of oil droplet sizes entering the filter cell was measured using a TSI scanning mobility particle sizer (SMPS) as indicated in Figure 3. The SMPS consists of a condensation particle counter (TSI 3031) and a differential mobility analyzer (DMA 3081). These allow measurements of the size distribution and number concentration of oil droplets in the air stream. The differential mobility analyzer is a continuous-flow analyzer that separates particles according to their electrical mobility in air. The DMA operates in the range of particle diameters from 10 nm through 1 μm. The droplets that exited the filter cell were carried away by a weak vacuum system.

Figure 4 shows the design of the filter cell. A network of nanofibers was placed on a washer and a transparent tape with a circular hole was used to keep the fibers attached to the washer. To make the cell airtight, a glass cover slide was held onto the top of the cell with grease. The flow path was from the inlet on the left to the outlet on the right. The oil fog flowed past the nanofibers and exited through the space between the cover glass C and the top of the tape E. The fog flow was practically normal to the plane containing nanofibers, which prevented transport of liquid between drops on the fibers, and no films covering them were visible in the present case. This filter cell allows the use of a high magnification objective lens to observe the capture and accumulation of oil droplets on the nanofibers. The distance between B and C was kept small so that the high power objective lens could be used.

Results and Discussion

Growth rate of a single drop

The experimental data for the growth of five different drops on a single nanofiber are shown in Figure 5. The experimental data for the drop growth were obtained by analyzing the micrographs using ImageJ software. Our optical measurements were able to reveal changes as small as 50 nm in the diameter of a drop on a nanofiber, after the drop diameter was larger than the diameter of the supporting nanofiber. There is a definite size above which the first drop on the fiber becomes visible to a human eye and that time is considered as time zero in Figure

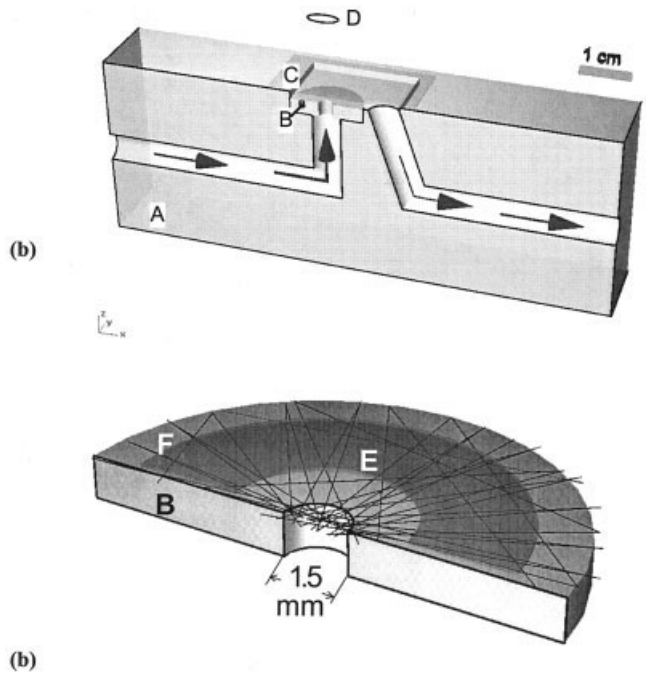

Figure 4. (a) Filter cell and (b) washer details, for observation of coalescence and collection of oil droplets on nanofibers.

A: Filter cell; B: washer; C: cover slip; D: objective lens of optical microscope; E: transparent tape with a center hole; F: nanofibers network.

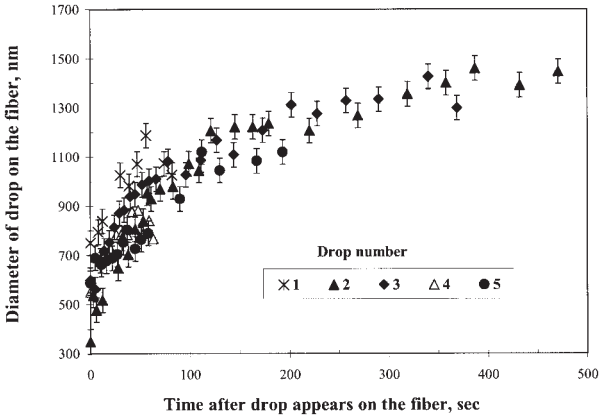

Figure 5. Diameter of individual drops growing on a nanofiber as a function of time.

5. Then, at about 10 s the droplet size becomes more than twice the nanofiber diameter. From that time on, the theoretical assumption that the nanofiber does not disturb the flow and droplet deposition near most of the droplet surface becomes sufficiently accurate. Moreover, because the theory predicts that $da/d(t-\tau) = \infty$ at $t - \tau = 0$, the data corresponding to the initial 10 s in Figure 5 are not significant. Droplet collection on nanofibers is shown in Figure 6, which shows a sequence of micrographs recorded by a video camera. The pictures shown are at times 0, 1, 10, 30, 60, and 120 min. The average velocity of the stream passing through the hole in the washer for the flow rate of 0.1 L/min was 0.84 m/s. The average drop diameter increased to 1.5 μm in 500 s.

The SMPS measurements gave the size distribution of oil droplets entering the filter cell. Figure 7 shows the results for the number of droplets per cm^3 plotted against the oil droplet size. Based on Figure 7, the probability distribution of droplet diameter for different temperatures of the oil pot was plotted as

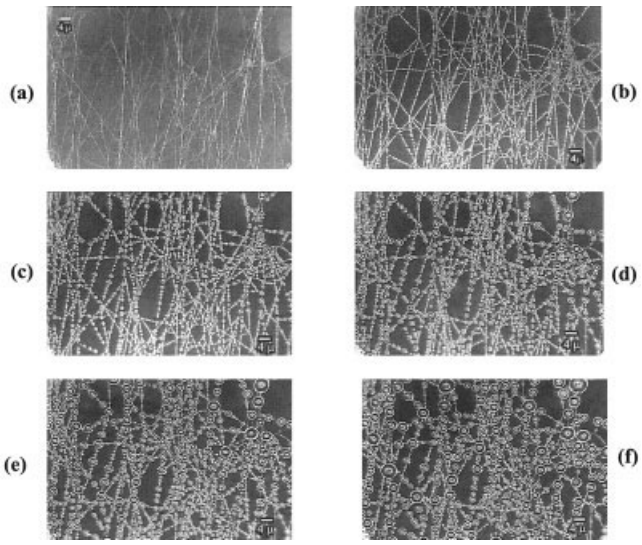

Figure 6. Frames from the movie of growth of oil drops on nanofiber network.

(a) Before the tiny oil droplets passed through the network. (b) After the tiny oil droplets passed through for 1 min, 10 min (c), 30 min (d), 60 min (e), and 120 min (f).

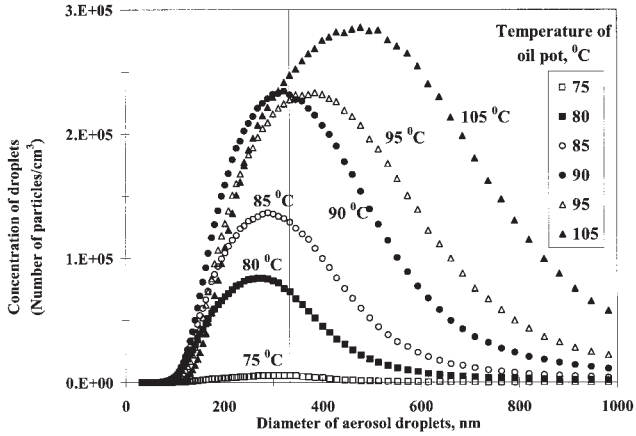

Figure 7. Scanning mobility particle sizer measurements of stream entering the filter cell at different oil pot temperatures.

shown in Figure 8. The vertical lines in Figures 7 and 8 correspond to a fiber diameter of 333 nm. The maximum in Figure 8 corresponds to the droplet diameter with the greatest population. The oil pot temperature of 95°C was selected for the drop growth rate experiments. For further experiments on droplet deposition, the oil pot was cleaned. This had an effect on the droplet-size distribution measured at 95°C: the distribution at 95°C shown in Figure 9 depicts lower concentrations, at the same most frequently observed diameter (cf. with the distribution for 95°C in Figure 7).

Based on the distribution of Figure 9, the concentration c was estimated by taking a summation of all data points, $c = 3.19 \times 10^6$ number of particles/cm^3. Also the number- and volume-average droplet diameters of the distribution were calculated to be 365 and 592 nm, respectively. It was observed that the larger droplets of sizes near 1000 nm may be few in number but they significantly affect the volume-average diameter.

The gas temperature was close to the room temperature (T = 300 K). The dynamic and kinematic viscosities of air are taken as $\mu = 1.7 \times 10^{-5}$ kg m^{-1} s^{-1} and $\rho = 1.11$ kg/m^3. For droplet diameter 592 nm and drop diameter 1500 nm, the Reynolds

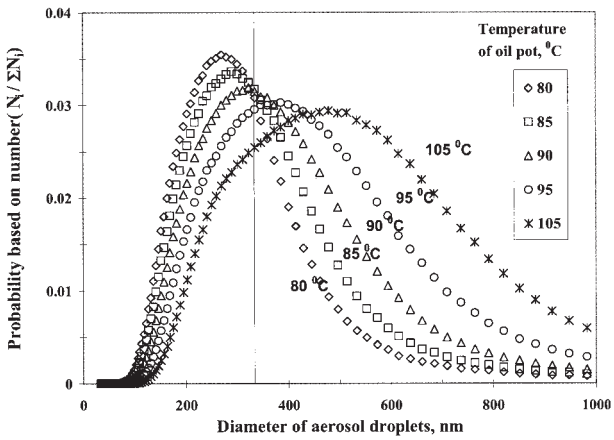

Figure 8. Probability distribution plot based on Figure 7 at different oil pot temperatures.

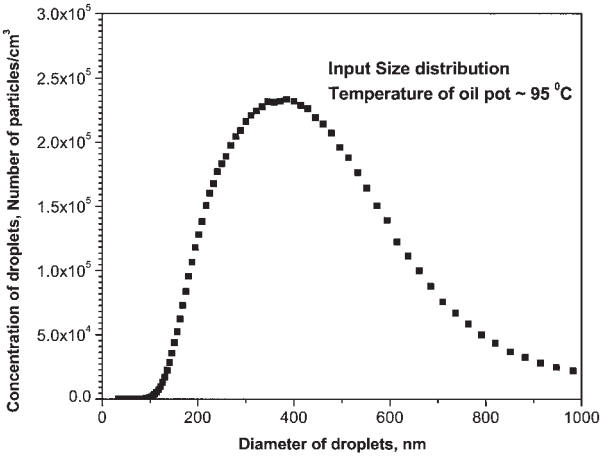

Figure 9. SMPS measurement of stream entering the filter cell.

numbers are Re = (3.55–8.99) $\times 10^{-2}$, Re $\ll$ 1, respectively, which implies that the viscous forces are predominant at both the droplet and the drop. In fact, the flow is a creeping flow. The diffusion coefficient is given by the Einstein formula (Eq. 28), where δ is the average radius of oil droplets in the gas flow, which yields $D = 4.37 \times 10^{-11}$ m^2/s for $2\delta = 592$ nm. Also the Peclet number, Pe $= 2.88 \times 10^4$, is much larger than one (Pe $\gg$ 1) for drop diameter $2a = 1500$ nm (cf. Figure 5). These conditions correspond to three of the models considered:

(1) Interception mechanism in creeping flow, Eq. 24

(2) Brownian diffusion in creeping flow for Pe $\gg$ 1, Eq. 35

(3) Vapor deposition by diffusion in creeping flow, Eq. 44

The stream of oil fog entering the filter cell was near room temperature. Under such conditions the saturation vapor pressure of oil is about 0.08 mmHg (as for propylene glycol), which corresponds to a volume fraction of vapor near the drop surface of the order of 0.08/760 $\approx 10^{-4}$. Then the average volume fraction of vapor in air flow is not more than $c_1 = (4/3)\pi\delta^3 c \times 10^{-4} \approx 3.46 \times 10^{-11}$. Taking for the estimate $D_v \approx 10^{-5}$ m^2/s, we obtain from Eq. 44 that the time required for growth of a drop of nearly 1 μm is about $t - \tau = 10^5$ s. This is much longer than the times of about 10^2 to 10^3 s observed in the experiment (Figure 6). Therefore, under the experimental conditions used the vapor deposition diffusion mechanism cannot be the growth mechanism.

The result of the calculations of drop growth based on the interception mechanism (Eq. 24), Brownian diffusion mechanism (Eq. 35), and a combination of these mechanisms (both Eqs. 23 and 34) were plotted for the number-average diameter (365 nm; Figure 10) and volume-average diameter (592 nm; Figure 11). The combined mechanism was modeled by assuming the two mechanisms are independent and weighted with parameters K_1 and K_2, respectively. Combining Eq. 23 and Eq. 34, we thus obtain the following differential equation

$$\frac{da^3}{dt} = K_1 1.5\pi U c \delta^5 + K_2 4 \frac{\pi}{2^{2/3}} a^{4/3} D^{2/3} U^{1/3} c \delta^3 \qquad (60)$$

where K_1 and K_2 are the weighting parameters constrained by

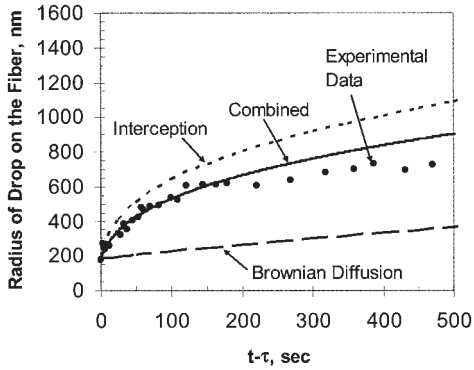

Figure 10. Comparison between experimental and predicted values of drop radius on a nanofiber as a function of time based on number-average diameter.

The data points are from the experiments. The curves are the calculated values for the interception mechanism for creeping flow and for the Brownian diffusion mechanism for Pe $\gg$ 1. The combined mechanism curve is for values of $K_1 = 0.55$ and $K_2 = 0.45$ with a regression coefficient value $R^2 = 0.97$.

$$K_1 + K_2 = 1 \qquad (61)$$

The combined mechanism results were obtained by numerically solving Eq. 60. The data for drop 2 in Figure 5 were used as the experimental data for comparison of the predicted and the experimental data. The values $K_1 = 0.55$, $K_2 = 0.45$ provided the best fit of the theory to the experimental data for the combined mechanism of droplet growth based on the number-average diameter. The values of K_1 and K_2 show that in this case the interception and Brownian diffusion mechanisms appear to be equally important. For volume-average diameter the values of $K_1 = 0.04$, $K_2 = 0.96$ best fit the predicted data to the experimental data. In the latter case the interception mechanism appears to make an insignificant contribution. The reason

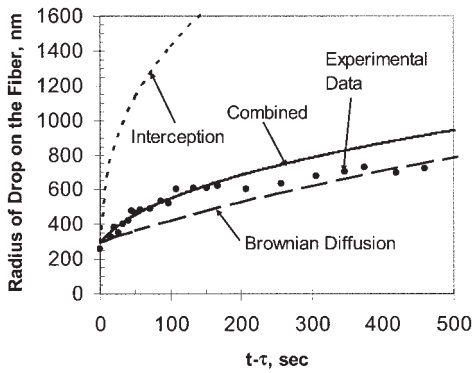

Figure 11. Comparison between experimental and predicted values of drop radius on a nanofiber as a function of time based on volume-average diameter.

The data points are from the experiments. The curves are the calculated values for the interception mechanism for creeping flow and for the Brownian diffusion mechanism for Pe $\gg$ 1. The combined mechanism curve is for values of $K_1 = 0.04$ and $K_2 = 0.96$ with a regression coefficient value $R^2 = 0.94$.

that the interception mechanism in the creeping flow is so sensitive to the value of δ is clear from Eq. 60 where it brings $da^3/dt \sim \delta^5$, whereas the Brownian diffusion is only about δ^3. Therefore, even a few bigger droplets in the fog, which substantially distort the volume average value of δ, lead to a significant overshoot in the value of da^3/dt. Suppression of this overshoot by a low value of the "weight" coefficient K_1 is nonphysical. Note that the regression correlation coefficient R^2 calculated in all the cases is based on data measured at time $<$ 200 s. The reasons for the experimental data being smaller than the predicted growth rate at longer times are not known. A nearly monodisperse distribution of droplet sizes is required to make a sharper distinction between the mechanisms.

Merging time for coalescence process

For the observation of merging drops, a high-speed camera (Redlake Imaging MotionScope®) was used to record the images from the microscope. The images were captured at the rate of 4000 frames per second (fps). The results obtained for drop merging on a nanofiber are shown in Figure 12. As can be seen from Figures 12A and 12B, during drop merging the drop size increased for the smaller drop as the drop size decreased for the larger drop.

For oil drops, as mentioned earlier, the Ohnesorge number was found to be much greater than one, which means that viscous effects dominate inertial and surface tension effects. The merging time t_* of two drops when viscous effects are dominant can be predicted using Eq. 58. Table 1 shows the comparison between the experimental and the predicted merging times. Experimental time was calculated based on two frames (Figure 12) at the rate of 4000 fps. The observed merging time is similar to that predicted by the model.

In these experiments, intense light was required because the shutter speed was very fast. Also the moment at which the picture is taken has to be very precise because it is possible to record a maximum of only 2 s for each attempt. The experiment can give more accurate results by increasing the frame rate or by using a more viscous fluid to lengthen the merging time.

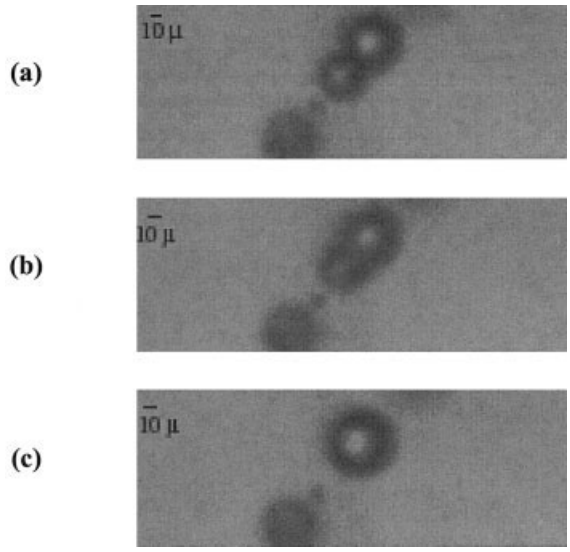

Figure 12. Consecutive video frames of two drops as they merged on microfiber at (a) 0 ms, (b) 0.25 ms, and (c) 0.5 ms.

The video was taken at the rate of 4000 fps.

Table 1. Merging Time for Droplets on Microfibers

Radius of Merging Drop a_0 (cm)	Ohnesorge Number	Predicted Merging Time (s)	Experimental Merging Time (s)
0.001686	54.8	4.8×10^{-4}	5×10^{-4}

Motionless drops on nanofibers shown in Figure 6 do not exhibit any instabilities. The merging drops in Figure 12 also do not exhibit any visible instability. The absence of any instabilities near the contact lines of drops moving over fibers is also fully corroborated by the images in Figure 2 in Yarin et al.[24]

Conclusions

(1) The drop growth mechanism on a nanofiber can be attributed to both interception and Brownian diffusion mechanism in the creeping flow conditions. Measurement of the exact contribution of both Brownian and interception mechanisms requires an almost monodispersed distribution of droplet sizes.

(2) Merging of two drops of mineral oil, which had a viscosity of 10 g cm^{-1} s^{-1} after they came into contact required about 0.5 ms. The observed merging time for two drops on a nanofiber was comparable to the predicted time from a simple fluid mechanical model.

Acknowledgments

This research was supported by the Coalescence Filtration Nanomaterials Consortium (Ahlstrom, Donaldson Company, Fleetguard, Hollingsworth and Vose, and Parker Hannifin) and by National Science Foundation Grant CTS-0310429.

Literature Cited

1. Doshi J, Reneker DH. Electrospinning process and applications of electrospun fibers. *J Electrostat.* 1995;35:151-160.
2. Reneker DH, Chun I. Nanometer diameter fibers of polymer produced by electrospinning. *Nanotechnology*. 1996;7:216-223.
3. Reneker DH, Yarin AL, Fong H, Koombhongse S. Bending instability of electrically charged liquid jets of polymer solutions in electrospinning. *J Appl Phys.* 2000;87:4531-4547.
4. Sherony DF, Kointner RC, Wasan DT. Coalescence of secondary emulsions in fibrous beds. In: Matijevic E, ed. *Surface and Colloid Science*. New York, NY: Plenum Press; 1978:99-160.
5. Pich J. Theory of aerosol filtration by fibrous and membrane filters. In: Davis CN, ed. *Aerosol Science*. New York, NY: Academic Press; 1966:223-280.
6. Tien C. *Granular Filtration of Aerosols and Hydrosols*. Boston, MA: Butterworths; 1989.
7. Brown RC. *Air Filtration: An Integrated Approach to the Theory and Application of Fibrous Filters*. Oxford, UK: Pergamon Press; 1993.
8. Sareen SS, Rose PM, Gudesen RC, Kintner RC. Coalescence in fibrous beds. *AIChE J.* 1966;12:1045-1050.
9. Spielman LA, Goren SL. Theory of coalescence by flow through porous media. *Ind Eng Chem Fundam*. 1972;11:66-72.
10. Bitten JF. Coalescence of water droplets on single fibers. *J Colloid Interface Sci.* 1970;33:265-271.
11. Rosenfeld JI, Wasan DT. Coalescence of drops in a liquid–liquid dispersion by passage through a fibrous bed. *Can J Chem Eng*. 1974; 52:3-10.
12. Briscoe BJ, Galvin KP, Luckham PF, Saeid AM. Droplet coalescence on fibers. *Colloids Surf.* 1991;56:301-312.

13. Raynor PC, Leith D. The influence of accumulated liquid on fibrous filter performance. *J Aerosol Sci.* 2000;31:19-34.
14. Blevins RD. *Applied Fluid Dynamics Handbook*. New York, NY: Van Nostrand Reinhold; 1984.
15. Johnson RW. *The Handbook of Fluid Dynamics*. New York, NY: CRC Press; 1998.
16. Yarin AL, Koombhongse S, Reneker DH. Bending instability in electrospinning of nanofibers. *J Appl Phys.* 2001;89:3018-3026.
17. Ye H, Naguib N, Gogotsi Y. TEM study of water in carbon nanotubes. *JEOL News* 2004;39:38-43.
18. Yarin AL, Yazicioglu AG, Megaridis CM. Thermal stimulation of aqueous volumes in carbon nanotubes: Experiment and modeling. *Appl Phys Lett*. 2005;86:013109/1-013109/3.
19. Batchelor GK. *An Introduction to Fluid Dynamics*. Cambridge, UK: Cambridge Univ. Press; 1994.
20. Clift R, Grace JR, Weber ME. *Bubbles, Drops and Particles*. New York, NY: Academic Press; 1978.
21. Frenkel J. Viscous flow of crystalline bodies under the action of surface tension. *J Phys USSR.* 1945;9:385-391.
22. Boucher DF, Alves GE. Dimensionless numbers. *Chem Eng Prog*. 1959;55:55-64.
23. de Gennes PG, Brochard-Wyart F, Quere D. *Capillarity and Wetting Phenomena. Drops, Bubbles, Pearls, Waves*. New York, NY: Springer-Verlag; 2004.
24. Yarin AL, Liu W, Reneker DH. Motion of droplets along thin fibers with temperature gradient. *J Appl Phys.* 2002;91:4751-4760.
25. Koombhongse S, Liu W, Reneker DH. Flat polymer ribbons and other shapes by electrospinning. *J Polym Sci Part B: Polym Phys.* 2001;39: 2598-2606.
26. Liu W, Wu Z, Reneker DH. Structure and morphology of poly(metaphenylene isophthalamide) nanofibers produced by electrospinning. *Polym Prepr* (*Am Chem Soc, Div Polym Chem*). 2000;41:1193-1194.

Manuscript received July 22, 2004, and revision received May 31, 2005.